nature electronics

ARTICLES

https://doi.org/10.1038/s41928-018-0148-3

Corrected: Publisher Correction

Integrated microthermoelectric coolers with rapid response time and high device reliability

Guodong Li[1,4*], Javier Garcia Fernandez[1,4], David Alberto Lara Ramos[1,2,3], Vida Barati[1,2], Nicolás Pérez[1], Ivan Soldatov[1], Heiko Reith[1], Gabi Schierning[1] and Kornelius Nielsch[1,2]

Microthermoelectric modules are of potential use in fields such as energy harvesting, thermal management, thermal imaging and high-spatial-resolution temperature sensing. In particular, microthermoelectric coolers (μ-TECs)—in which the application of an electric current cools the device—can be used to manage heat locally in microelectronic circuits. However, a cost-effective μ-TEC device that is compatible with the modern semiconductor fabrication industry has not yet been developed. Furthermore, the device performance of μ-TECs in terms of transient responses, cycling reliability and cooling stability has not been adequately assessed. Here we report the fabrication of μ-TECs that offer a rapid response time of 1 ms, reliability of up to 10 million cycles and a cooling stability of more than 1 month at constant electric current. The high cooling reliability and stability of our μ-TEC module can be attributed to a design of free-standing top contacts between the thermoelectric legs and metallic bridges, which reduces the thermomechanical stress in the devices.

Microthermoelectric modules are capable of generating electricity from waste heat (a microthermoelectric generator, μ-TEG) or alternatively using electricity to generate cooling to locally manage heat (a microthermoelectric cooler, μ-TEC). They could be important components in a range of emerging systems, including thermally integrated energy-autonomous devices[1,2], spatially defined and dynamically temperature-controlled lab-on-a-chip devices[3,4], biomedical devices[5–7], the Internet of Things devices[8] and wearable electronics[9,10]. Being smaller in leg cross-sections and shorter in leg height, these micromodules can be easily integrated with multifunctional devices and present distinct advantages over large generators and coolers. In particular, they can generate electricity from a tiny temperature gradient (such as from the human body)[11], they can handle heat fluxes up to several hundred W cm^{-2} (ref. [12]), they have fast response times and good device reliability[13,14], they can work as temperature sensors and controllers with high spatial resolution[4], and they allow microscale device integration to be used in flexible electronics[15].

The fabrication of modern electronic devices relies on microelectromechanical system (MEMS) technology to create miniature functional units such as sensors, actuators and converters, which can be integrated on-chip and commercialized at low cost. Industrial applications of microthermoelectric modules thus require a fabrication route that is MEMS-compatible and cost-effective. Electrochemical deposition (ECD) of metals and contact materials is the standard back-end-of-line (BEOL) process for integrated circuits in complementary metal-oxide semiconductor (CMOS) technologies[16]. Compared to other deposition techniques (such as physical evaporation, sputtering or electron-beam deposition), ECD has many inherent advantages, including adjustable material compositions through modification of the electrolyte, large scalability and a high material deposition rate that enables thick-film deposition of up to tens of micrometres[17,18]. Therefore, the development of a MEMS-compatible ECD process for functional thermoelectric materials was a key step in enabling on-chip integration of thermoelectric modules[12,19]. However, the potential of scaling up existing approaches remains challenging due to factors such as complex device fabrication routes, limited device efficiency and the instability of ECD material properties[2].

A cost-effective fabrication route is not the only requirement for the commercialization of microthermoelectric modules, either as TEGs or TECs—detailed device performance characterization is just as important. For example, a fast device response time, as well as good device durability, are prerequisites for applications in the physical sciences such as stabilizing the optimal working temperature of an on-chip-integrated laser diode[20], or applications in the biological sciences such as dynamic cell stimulation and long-term cell cultivation[21]. So far, however, the transient responses, cycling reliability and long-term stability of microthermoelectric modules have not been fully characterized.

In this Article, we report the fabrication of an integrated μ-TEC module using ECD bismuth tellurium (BiTe) compounds and a detailed characterization of the device. The μ-TEC offers an extremely fast cooling response of <1 ms, a device reliability of up to 10 million cooling cycles and a long-term cooling stability of more than 30 days under constant electric current.

Fabrication process for improved integrated μ-TECs

Since the end of the last century, several fabrication routes have been proposed for the development of miniature thermoelectric modules. Kishi and colleagues[11] demonstrated a millimetre-sized, 600-μm-high thermoelectric module by mechanically cutting and micro-bonding sintered BiTe compounds. Using this design it was possible to realize a cooler with a maximum temperature difference of 61.3 K and heat absorption of 0.36 W. Stordeur and Stark[22] reported a design of an in-plane thin-film thermoelectric module in which stripes of thermoelectric materials of n-type $Bi_2(Se_{0.1}Te_{0.9})_3$ and p-type $(Bi_{0.25}Sb_{0.7})_2Te_3$ were sputtered via magnetron onto a polyimide foil substrate. The flexible polyimide foil was later packed together to form a 3-mm-high segment TEG with a power

[1]Institute for Metallic Materials, IFW Dresden, Dresden, Germany. [2]Institute for Materials Science, Dresden University of Technology, Dresden, Germany. [3]Consejo Nacional de Ciencia y Tecnologia, Del. Benito Juárez, Ciudad de Mexico, Mexico. [4]These authors contributed equally: Guodong Li and Javier Garcia Fernandez. *e-mail: g.li@ifw-dresden.de

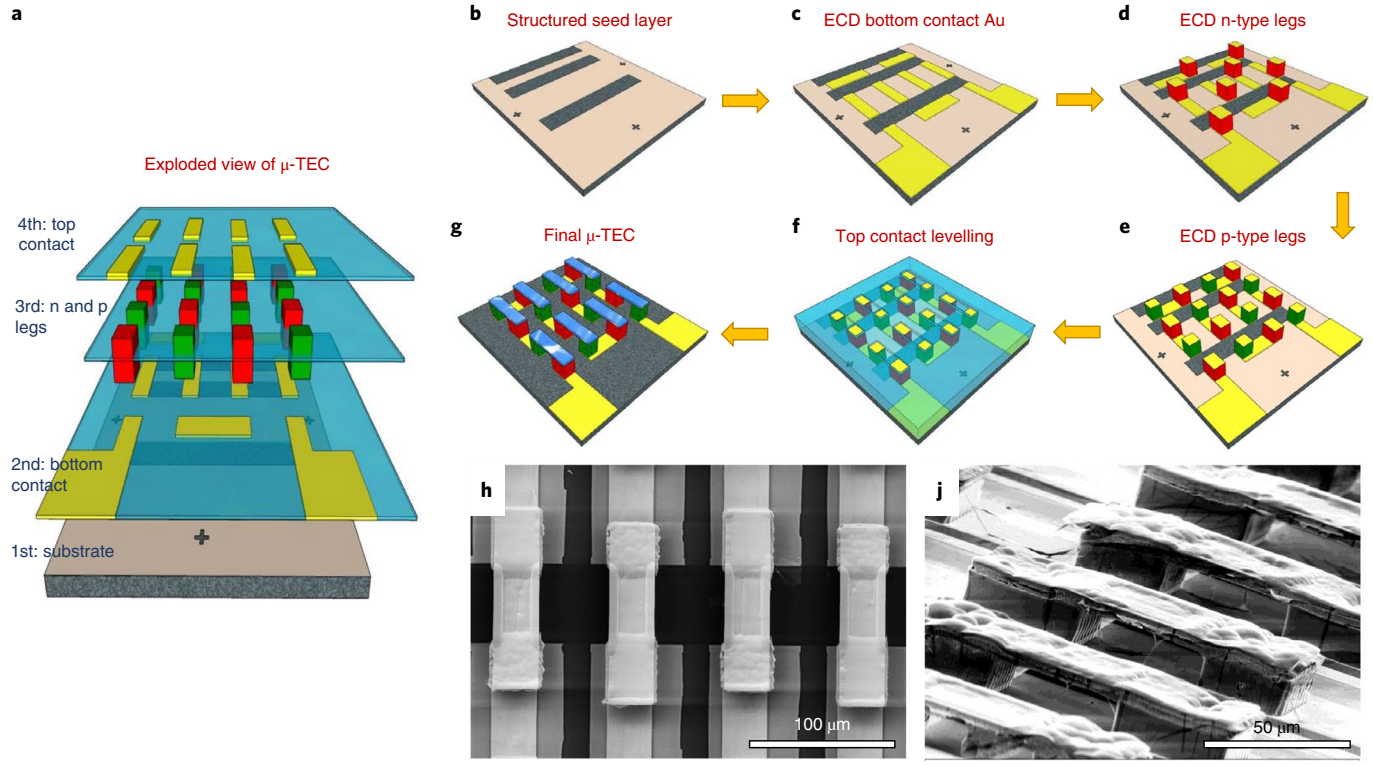

Fig. 1 | Schematic fabrication line for integrated μ-TECs and corresponding secondary electron images. a, Exploded view of an integrated μ-TEC with six leg pairs, demonstrating the four-layer structure. **b**–**g**, The μ-TEC device is fabricated using the following steps: coating the supporting Si/Si_3N_4 substrate with a Au seed layer (**b**), ECD of a 3 μm Au layer as bottom contact (**c**), ECD of 10 μm BiTeSe as n-type legs (**d**) and Te as p-type legs, followed by ECD of 1 μm Au protection on top (**e**), and top contact levelling by partially exposing thick photoresist (**f**), resulting in the final μ-TEC device (**g**). **h**,**j**, Top (**h**) and side (**j**) scanning electron microscopy views of the as-fabricated μ-TEC device.

output of a few tens of microwatts under a temperature difference of 20 K. However, both routes resulted in thermoelectric devices with heights not suitable for on-chip integrated applications such as local temperature management or higher-resolution temperature sensing. In view of these constraints, in 1998, Fleurial and colleagues[23] developed a pioneering approach to produce microthermoelectric modules by combining conventional photolithography and ECD techniques. The first as-fabricated TEG module consisted of 126 circular thermoelectric modules with a typical diameter of 60 μm and height of 20 μm (ref. [19]). Following this work, many studies have actively pursued the feasible and cost-effective fabrication of microthermoelectric modules based on MEMS-like technology[24–32]. However, due to the complex fabrication process during ECD and lithography, most fabricated TEGs suffer from large contact resistance and thus have relatively low efficiency.

To fabricate μ-TECs with advanced device characteristics, we combined standard photolithography and a modified ECD technique. The as-fabricated μ-TECs were composed of four vertical layers: the substrate, the bottom contact, the thermoelectric elements and the top bridge contact (Fig. 1a). To achieve this, we used multiple steps of photolithography and mask alignments (Figs. 1b–g and Supplementary Information for a detailed μ-TEC fabrication line). Starting with a silicon substrate with a 100-nm-thick insulating Si_3N_4 on top, a conducting seed layer of 5-nm-thick Cr and 100-nm-thick Au was first coated and structured, followed by a 3-μm-thick ECD Au layer as bottom contact for the thermoelectric elements. We then sequentially deposited 10-μm-thick n-type material ($Bi_2(Te_{0.95}Se_{0.05})_3$, abbreviated as BiTeSe) and p-type material (pure Te) by ECD into the photoresist cavities (see Methods). In contrast to other fabrication routes based on ECD, after each deposition of thermoelectric materials in our fabrication line the sample was immediately transferred to a bath of Au electrolyte, where a 1-μm-thick Au layer was electroplated on top of each leg. By doing so, the native surfaces of the thermoelectric elements were protected against oxidation during the following process, and intimate contacts between the Au and thermoelectric elements further reduced the contact resistivity, leading to a negligible contact resistance in the devices (Supplementary Fig. 2).

To build a top bridge contact, we developed a facile two-step lithography technique to level the leg pairs (Fig. 1f and Methods). We then electrochemically deposited another 6-μm-thick layer of Au as the top bridge contact. As the final step, the redundant conducting seed layer was chemically etched and all the photoresists were removed (Fig. 1g). The as-fabricated μ-TECs are vertically free-standing on the substrate, similar to commercial bulk Peltier coolers (Fig. 1h,j), and they can be categorized as a microscale cross-plane thermoelectric device. Here, the n-leg has a width of 30 μm and a length of 40 μm, whereas the p-leg has square dimensions of $30 \times 30\,\mu m^2$. Within a $2 \times 2\,mm^2$ substrate area, we have integrated 220 leg pairs, resulting in a packing density of 5,500 leg pairs per cm^2 and a fill factor of around 20% (Supplementary Fig. 1).

The as-fabricated μ-TECs exhibit very small intrinsic device resistance. We investigated the electrical transport characteristics of the as-fabricated μ-TECs by plotting the electrical resistance measured for an increasing number of leg pairs within one thermoelectric module (Supplementary Fig. 3a). The measured resistance scales linearly with the number of legs, and by fitting the data to a straight line we obtained an average resistance of 1.05 Ω for each leg pair. Given that thick bottom (3 μm) and top (6 μm) Au contacts were used in the μ-TEC, the resistance contribution from the Au

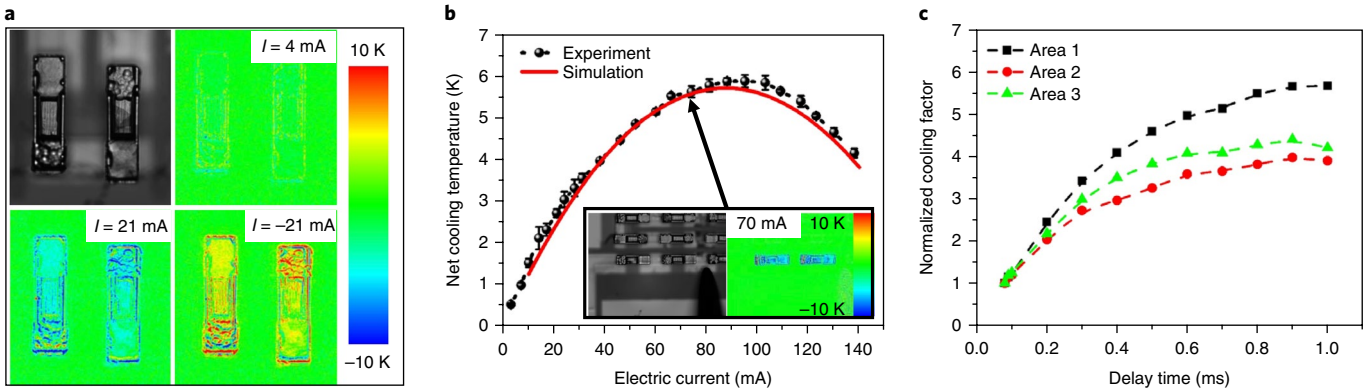

Fig. 2 | Cooling performance of μ-TECs. a, Optical microscopy image of an integrated μ-TEC device and thermoreflectance images with applied electric currents of 4, 21 and −21 mA. **b**, Net cooling temperature of two leg pairs in the electric current range 5–140 mA at room temperature (~20 °C) and in an ambient environment. Inset: optical and thermoreflectance images with an applied electric current of 70 mA. Error bars were calculated by averaging all pixels in the n-leg and bridge area. The red curve shows the COMSOL simulation result. **c**, Dependence of normalized cooling factor on specific delay time, measured after switching on the electric current of 70 mA for three different areas of μ-TECs: n-leg of cooler 1 (black), bridge of cooler 1 (green) and n-leg of cooler 2 (red). The dashed lines are guides to the eye.

contacts is negligible (~0.016 Ω per leg pair). The experimentally obtained resistance per leg pair is also consistent with the theoretical expected values, which are estimated to be around 1 Ω based on the reported electrical conductivities of ternary BiTeSe (ref. [18]) and pure Te (ref. [33]). Additionally, the I–V characteristic of the complete device shows excellent ohmic behaviour (Supplementary Fig. 3b). These results show that the fabricated μ-TECs have ohmic contact interfaces with negligible resistance.

Net cooling and transient response time of μ-TECs

To characterize the cooling performance of the as-fabricated μ-TECs, we first carried out charge-coupled-device (CCD) based thermoreflectance microscopy measurements (see Methods for details) under three different electric currents (Fig. 2a). In an ambient environment (room temperature, around 20 °C), when a small electric current of 4 mA was applied to the whole integrated μ-TECs we could barely observe any cooling effect. When we increased the electric current to 21 mA we found significant cooling with a net temperature change (ΔT) of around −4 K. Conversely, when we switched the electric current polarity, we observed significant heating with a ΔT of around 3 K on top of the leg pairs. In addition, to investigate the cooling homogeneity of our integrated μ-TECs we performed thermoreflectance measurements on various areas of the entire integrated devices under an electric current of 50 mA. Six different areas were investigated in detail, and relatively homogeneous cooling (over 80%) was realized in these areas (Supplementary Fig. 4).

To comprehensively characterize the cooling dependence on the applied electric currents and the transient cooling response of the as-fabricated μ-TECs, we performed detailed thermoreflectance characterization on two leg pairs connected in series in an ambient environment. For thermoreflectance measurements, a pulsed electrical current (1.5 ms on and 4.5 ms off) was applied, and the induced temperature changes were averaged for at least 100 s to enhance the measurement accuracy. With an increase of electric current from 5 to 140 mA, the net cooling of the two leg pairs first increased gradually to a peak value of 6 K at around 100 mA, and then dropped when the current was further increased (Fig. 2b). The typical dependence of net cooling on electric currents reveals two competing mechanisms in the μ-TEC: on the one hand the charge carriers take heat away from the top bridge (Peltier cooling effect), and on the other hand they also heat up the whole system (Joule heating effect), especially when the electric current is larger than 100 mA, where Joule heating starts to play an important role and decreases the overall cooling performance.

To investigate the transient cooling response (how fast the device reacts to the applied electric current), we applied a pulsed electrical current (1.5 ms on and 4.5 ms off) and measured the net cooling of the leg surfaces at different times after switching on the current (delay times). Considering the time constant of Peltier cooling and the Joule effect (in the range of 0.1 ms)[34], an initial delay time of 0.1 ms was selected. We observed that the net cooling did not increase after 0.9 ms (Fig. 2c) and stable net cooling could be reached within 1 ms for several different μ-TECs. The response time of our μ-TECs is one order of magnitude shorter than that of a similar μ-TEC (20 ms, ref. [14]) and three orders of magnitude shorter than the response time of 8 s for the smallest commercial Peltier device[14]. The rapid cooling response in our μ-TECs can be attributed partly to the shorter leg heights and partly to a better electrical and thermal contact between the Au electrode and thermoelectric elements, which is a result of the immediate Au deposition after each ECD for the thermoelectric elements.

Durability of μ-TECs

To assess the durability of the μ-TECs we investigated the cooling stability of two in-series-connected μ-TECs with constant direct current, as well as their cycling reliability with a pulsed electric current. In the cooling stability experiment, a constant direct current of 70 mA was continuously applied to the μ-TECs under an ambient environment, and the thermoreflectance measurements were performed at certain time intervals, as indicated by the measurement points in Fig. 3a. The net cooling of our μ-TECs was stable over the whole period of 30 days—four times larger than the previous record[14]. Note that the relatively big variations in net cooling over periods of 200 and 300 h were related to a loose contact between the measurement probes and contact electrodes. Meanwhile, we also monitored the resistance change in the two μ-TEC leg pairs during the long-term stability measurements and observed a resistance increase from an initial 3.16 Ω to 5.21 Ω by the end of the measurement (Fig. 3a). The increase in device resistance might be attributed to Au atom diffusion in the thermoelectric legs, which may happen when a high constant electric current is applied for a long time. To mitigate Au atom diffusion in future devices and further increase the cooling stability of the μ-TEC, a thin barrier/block layer, such as nickel (Ni) or chromium (Cr), could be placed between the thermoelectric material and top electrode[35].

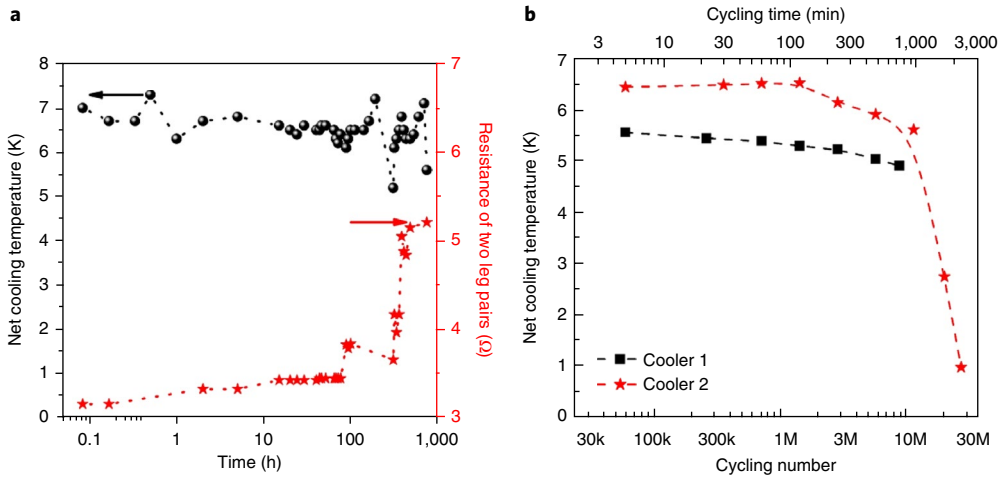

Fig. 3 | Durability of μ-TEC devices. a, Long-term cooling stability test of two in-series-connected μ-TECs with a constant applied current of 70 mA. The black dots represent the net cooling temperature and the red stars represent the total resistance of the two μ-TECs. **b**, Cycling reliability of μ-TECs with cooling pulses (1 ms on and 4 ms off), represented as the cooling temperature as a function of cycling number and cycling time for two separated experiments. In each experiment, two in-series-connected leg pairs were investigated: cooler 1, from the first experiment (black squares), and cooler 2, from the second experiment (red stars). The dashed lines are guides to the eye.

To examine cycling reliability we applied a pulsed current (1 ms on and 4 ms off) to another two in-series-connected μ-TEC leg pairs for 30 million cycles. Two separate experiments were performed, and the net cooling was measured by thermoreflectance microscopy with increasing time intervals, seven to nine times during the experiments (Fig. 3b). The μ-TECs showed a constant cooling ability up to 10 million cycles. Although such a high cycling reliability has not been documented for μ-TECs, we expect even higher cycling numbers could be reached if a longer pulse period were applied. With 200 cooling and heating cycles in a single second of our current measurements, extraordinary robust electrical and thermal contacts must have been realized between the legs and suspended bridges in our μ-TECs. Again, such a high cycling reliability of our μ-TECs is another result of the immediate Au deposition onto each thermoelectric element. Device degradation started to appear when the cycling number was more than 10 million, and after this investigation all the in-series connected μ-TECs were dead due to loose contact between the legs and the suspended bridges. We speculate that one direct reason for the failure of the contacts might be the different thermal expansion coefficients of the top metallic bridge and thermoelectric legs.

Note that our current as-fabricated μ-TECs are not sealed/covered by a top plate, as is typically done in conventional Peltier modules. Instead, they are vertically free-standing on the supporting substrate (Fig. 1j). This free-standing design of the μ-TEC, without being fixed on the top bridges, provides the μ-TECs with some freedom to adapt to possible displacements and internal strain (a so-called 'breathing' process) caused by misfits of the material thermal expansion coefficients, especially during the cycling reliability test. Although this design feature is key for realizing the extraordinarily high cycling stability, a soft and thick polymer that is electrically and thermally insulating, such as polydimethylsiloxane (PDMS), could be used to seal the entire integrated μ-TECs to better prepare our devices for applications. Conversely, as for the top plates, materials that are thermally conductive and mechanically stiff, such as lightweight ceramic plates, could be placed on top of the sealed μ-TECs. It is worth noting that either the polymer filling or a top-plate attachment to the μ-TECs would increase the system thermal mass, and will thus lead to a longer response time.

Temperature-dependent cooling properties of μ-TECs

A promising application for μ-TECs is to integrate them with some overheating functional devices that need on-chip cooling or thermal stabilization, such as in an integrated optoelectronic device, where the active photonic component requires highly precise temperature control. In this case, μ-TECs with a Π−shaped geometry can be built around the overheating laser diode and provide active cooling through the supply of an electric current[20,36]. Because the properties of a thermoelectric material are temperature-dependent, we further characterized the cooling performance of our μ-TECs at different substrate temperatures. The measurements were performed at constant electric current (70 mA) and in an ambient environment. A commercial Peltier element was used to control the base temperature of the μ-TECs in the range 290–380 K. We found that the net cooling substantially increased with increasing substrate temperature (Fig. 4). At 380 K, a net cooling of 12 K was achieved. This can be explained as follows. In the measured temperature range from 290 to 380 K, the overall thermoelectric properties of BiTe compounds are enhanced[37] and therefore higher cooling power can be achieved.

In addition, we performed thermoreflectance measurements at 280 K, where the base temperature of the μ-TECs is around 7 °C. As we applied the same pulsed electric current as above (70 mA, with pulse of 1 ms on and 4 ms off) to the μ-TECs, we observed periodic water condensation and desorbing on the bridge surfaces (Supplemental Video 1). This experiment shows direct evidence that our μ-TECs could be used as a water collector for potential microscale applications[38].

Model simulation and device optimization

For a TEC, the electric-current-dependent net cooling can be analytically analysed with the heat equation[39],

$$Q_c = S_{eff} \times I \times T_c - \frac{I^2 \times R_{eff}}{2} - K_{eff} \times \Delta T$$

where Q_c, I, T_c, S_{eff}, R_{eff} and K_{eff} are the cooling power, applied electric current, absolute temperature at the cold side, effective Seebeck coefficient ($S_{eff} = S_p - S_n$), effective resistance and effective thermal conductance of one leg pair, respectively. As $R_{eff} = 1.05\,\Omega$ has already

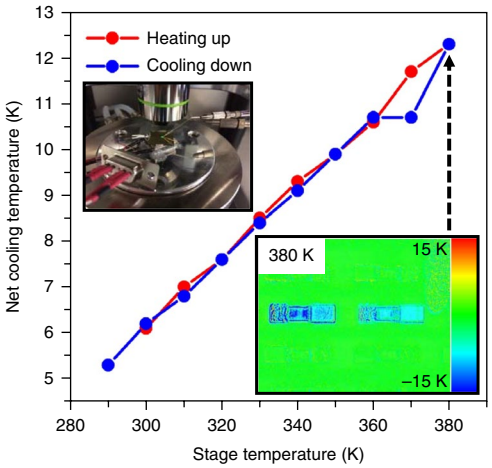

Fig. 4 | Temperature dependence of net cooling. Stage temperature-dependent cooling performance of two in-series-connected μ-TECs in an ambient environment with an applied electric current of 70 mA. Top inset: photograph of the μ-TEC sample mounted on a commercial Peltier element. Bottom inset: thermoreflectance image of two leg pairs at 380 K. The solid lines are guides to the eye.

been characterized (Supplementary Fig. 3a), $S_{eff} = 314\,\mu V\,K^{-1}$ and $K_{eff} = 718\,\mu W\,K^{-1}$ are calculated by fitting the experimental cooling performance (see Methods for details). For the value of S_{eff}, a possible Seebeck coefficient combination of $S_p = 234\,\mu V\,K^{-1}$ and $S_n = -80\,\mu V\,K^{-1}$ can be reasonably assumed for the p-type Te[33] and n-type BiTeSe[18], respectively.

Based on hints from the analytical analysis we simulated the cooling performance for one μ-TEC using a finite-element method (FEM)-based COMSOL simulation. In the simulation, we fixed the Seebeck coefficient values for each material as the values obtained from the above analytical simulation, and used a common effective thermal conductivity for both legs as an adjustable parameter to reproduce the experimental data. A good fit of the experimental data was achieved with a thermal conductivity value of ~3 $W\,m^{-1}\,K^{-1}$, as shown by the red solid line in Fig. 2b (for more details about the theoretical simulation see Supplementary Fig. 5). Our μ-TEC is, in principle, fabricated along the cross-plane direction of ECD materials, and the thermal conductivity value of 3 $W\,m^{-1}\,K^{-1}$ is in line with the literature values for the direction parallel to the *c* axis at room temperature[40]. We also learn from the COMSOL simulation that net cooling in our μ-TEC is possible only when the contact resistivity between the Au electrodes and thermoelectric elements is on the order of $10^{-11}\,\Omega\,m^2$. This negligible contact resistance can be attributed to our special ECD deposition route, in which the as-deposited thermoelectric legs are immediately covered by a thin layer of Au.

By using the effective Seebeck coefficient and thermal conductance, which we obtained from the analytical simulation, we could estimate that a heat absorption density of ~6.8 $W\,cm^{-2}$ is achieved in the maximum cooling regime (in the electrical current range of 70–100 mA). At the maximum cooling point, the coefficient of performance (COP) is calculated to be ~3.7%. To obtain an idea of the performance of our current microthermoelectric module as a generator, we also simulated the power output performance of our devices when used as power generators. With a temperature gradient of 6 K between the hot and cold sides, as we have observed in the thermoreflectance measurements, an output power density of 5.8 $mW\,cm^{-2}$ and an efficiency of 0.02% can be realized with our current design of μ-TEGs. Note that such a low efficiency is mainly due to the low device figure of merit (*ZT*) in our μ-TEGs ($ZT \approx 0.05$ at 293 K). With better materials used in the μ-TEGs, for example with a device *ZT* of 1 at 293 K, the efficiency can be enhanced to around 2% with the same temperature gradient of 6 K.

We assume that the cooling performance could be further enhanced by optimizing the device geometry. Based on the form factor[41], for the thermoelectric materials we are using in our devices, an optimized geometry would be 30 μm × 30 μm for the n-type BiTeSe and 30 μm × 115 μm for the p-type Te. With this optimized geometry design, for the μ-TECs we anticipate a cooling power density of 57 $W\,cm^{-2}$ and a COP of 7.4% at 293 K, and for the μ-TEGs we expect an output power density of 14.3 $mW\,cm^{-2}$ and an efficiency of 0.03% under the same conditions as above.

Conclusions

By combining a modified ECD process for thermoelectric thick films and standard photolithography techniques, we have fabricated integrated microthermoelectric devices with a packing density of 5,500 leg pairs per cm^2. In an ambient environment, a maximum net cooling temperature of 6 K is reached in the as-fabricated μ-TECs at room temperature, and the cooling performance can be further enhanced to more than 12 K when the substrate is heated to 380 K, as a target temperature of the thermal stabilization of optoelectronic components. The as-fabricated μ-TECs also show a rapid cooling response time of 1 ms and demonstrate a stable cooling performance over 30 days. Furthermore, a high reliability of more than 10 million cooling cycles is achieved.

Methods

Electrochemical deposition of n- and p-type thermoelectric materials. n-Type BiTeSe and p-type pure Te were electrochemically deposited at room temperature using a BioLogic VSP modular five-channel potentiostat/galvanostat via a pulsed deposition technique with a saturated Ag/AgCl reference electrode. For the n-type BiTeSe, the electrolyte was prepared by dissolving 10 mM TeO_2 (Merck, 99.5%) in 1 mol concentrated nitric acid (Merck, 69%), followed by the addition of 10 mM $Bi(NO_3)_3$ (Sigma Aldrich, 99.999%) and 1.1 mM SeO_2 (Strem Chemicals, 99.8%). For the p-type Te, 10 mM TeO_2 was dissolved in 1 M concentrated nitric acid. During the pulsed deposition of n-type material, the deposition potential (E_{on}) was −0.015 V with a pulse time (t_{on}) of 10 ms, followed by a reverse potential (E_{off}) of 0.186 V with an off pulse time (t_{off}) of 50 ms. With these deposition parameters for BiTeSe, we estimated the deposition rate to be ~0.27 μm per 1,000 pulse periods (or 0.27 μm min^{-1}). Similarly, for the p-type Te, conditions of $E_{on} = -0.075$ V with $t_{on} = 10$ ms and $E_{off} = 0.180$ V with $t_{off} = 50$ ms were used, and the deposition rate was ~0.13 μm per 1,000 pulse periods (or 0.13 μm min^{-1}). For both materials, compact legs were obtained and verified by secondary electron images.

Photolithography for photoresist levelling and the suspended bridge construction. A facile two-step lithography process was used to build the suspended bridges over the 10-μm-thick n- and p-type thermoelectric legs. In the first step, photoresist of AZ9260 (MicroChemicals) with a thickness of ~20 μm was spin-coated on the sample and the bridge areas were irradiated by a laser diode (μPG 101 from Heidelberg Instruments) with a small dose, so that only the top few micrometres (~7 μm) of photoresist was dissolved in the subsequent development process. With step-by-step control of the development process, the correct surfaces of the thermoelectric legs were obtained. Surface profile scanning with a Dektak profilometer was usually performed to ensure that a good levelling had been achieved in the legs and centre photoresist. Afterwards, a thin Au layer of ~10 nm was sputtered on the whole sample to serve as a seed layer and also as a stop layer for the subsequent lithography. In the second step, the same photoresist (AZ9260) was spin-coated on the entire sample, but with a thickness of 10 μm. A second photolithography stage was performed directly over the same bridge areas and these areas were fully developed. A thick Au layer of ~6 μm was then electrochemically deposited to form the bridges. In the final step, all photoresists were chemically stripped away and only bridges were kept intact, as shown by the secondary electron image in Fig. 1j.

CCD-based thermoreflectance microscopy measurement. This technique relies on measuring the relative change in the sample's surface reflectivity as a function of temperature, and our measured set-up was built by Microsanj (NT100) with a light-emitting diode wavelength of 530 nm. When an electric current is applied to a μ-TEC, charge carriers in the thermoelectric elements will either take heat away or eject heat to the suspended bridges, depending on the polarity of the electric current. The temperature change is proportional to the change of reflectivity and can be expressed as $\Delta T = \Delta R/(R_0 C_{th})$, where *R* and C_{th} are the thermal reflectivity and thermoreflectance coefficient of the surface material, respectively. To measure the net cooling temperature precisely, C_{th} was separately calibrated on reference

samples with Au surfaces, which were prepared by different deposition techniques (sputtered Au and ECD Au). For the sputtered Au surface, $C_{th} = -2.9 \times 10^{-4}\,K^{-1}$ whereas for the ECD Au, $C_{th} = -2.8 \times 10^{-4}\,K^{-1}$. In our measurements we used a value of $C_{th} = -2.8 \times 10^{-4}\,K^{-1}$ because our bridge surface is ECD Au. The p-type Te legs of our μ-TECs typically exhibit a rough surface (r.m.s. of ~1 μm), whereas the surface of the n-type BiTeSe legs and suspended bridges is relatively smooth. Because the thermoreflectance measurements are very sensitive to surface roughness, the cooling data were only extracted from the smooth areas, and the error bars were calculated by averaging all pixels in the relevant images.

For the cycling measurement, a pulsed electric current was continuously generated by a signal generator incorporated into the thermoreflectance set-up (Microsanj). Users can define the pulse time and the amplitude of the applied electric current. In this work, we set the electric current as 70 mA with a pulse time of 5 ms with 1:4 on/off ratio.

Analytical calculation and FEM simulation. In the analytical calculations, as a first approximation, the heat equation can be expressed as

$$\Delta T = \frac{S_{eff} \times I \times T_c - \frac{1}{2} I^2 \times R_{eff} - Q_c}{K_{eff}}$$

Given that the maximum temperature difference (ΔT_{max}) is achieved at the optimal current (I_{opt}) when $d(\Delta T)/dI = 0$, S_{eff} can be expressed as follows if one assumes that near this point dQ_c/dI is negligible (the amount of heat pumped due to the Peltier effect and lost heat due to Fourier conduction and Joule heating is balanced):

$$S_{eff} = \frac{I_{max} \times R_{eff}}{T_c}$$

where $I_{max} = 86$ mA, $T_c = T_0 - \Delta T = 293\text{K} - 6\text{K}$ and $T_0 = 293$K is the temperature at the hot side, which is equal to the ambient temperature under the assumption of a perfect heat sink. Moreover, at the lower current limit, where Joule heating is negligible, the temperature difference follows a linear behaviour with respect to the input current, with a slope proportional to the Peltier coefficient (Π): $Q = K_{eff} \times \Delta T = \Pi \times I$. Considering the second Thomson relation at mean temperature T_0, the effective thermal conductance of the μ-TEC can be written as

$$K_{eff} = \frac{S_{eff} \times T_0}{c}$$

where $c = 0.128\,\text{K mA}^{-1}$ is the slope of the ΔT versus I curve in the linear regime. Note that this analytical model just roughly estimates the thermoelectric properties of the device, which will be subsequently refined and validated with COMSOL FEM simulations.

FEM simulations were performed using a COMSOL software package. In the simulation, Seebeck coefficients of $234\,\mu\text{V K}^{-1}$ for the p-type Te and $-80\,\mu\text{V K}^{-1}$ for the n-type BiTeSe were assumed, respectively. For the electrical conductivity of each material, values of $1 \times 10^5\,\text{S m}^{-1}$ for the BiTeSe and $1.2 \times 10^4\,\text{S m}^{-1}$ for the Te were used (both of which are close to values reported in the literature[18,33]) to reproduce the total resistance of 1.05 Ω for one leg pair.

Data availability

The data that support the plots within this paper and other findings of this study are available from the corresponding author upon reasonable request.

Received: 20 July 2018; Accepted: 18 September 2018;
Published online: 12 October 2018

References

1. Twaha, S., Zhu, J., Yan, Y. & Li, B. A comprehensive review of thermoelectric technology: materials, applications, modelling and performance improvement. *Renew. Sustain. Energy Rev.* **65**, 698–726 (2016).
2. Yan, J., Liao, X., Yan, D. & Chen, Y. Review of micro thermoelectric generator. *J. Microelectromech. Syst.* **27**, 1–18 (2018).
3. Venkatasubramanian, R., Siivola, E., Colpitts, T. & O'Quinn, B. Thin-film thermoelectric devices with high room-temperature figures of merit. *Nature* **413**, 597–602 (2001).
4. Chowdhury, I. et al. On-chip cooling by superlattice-based thin-film thermoelectrics. *Nat. Nanotech.* **4**, 235–238 (2009).
5. Watkins, C., Shen, B. & Venkatasubramanian, R. Low-grade-heat energy harvesting using superlattice thermoelectrics for applications in implantable medical devices and sensors. In *Proc. ICT 2005, 24th Int. Conf. Thermoelectrics* 265–267 (IEEE, 2005).
6. Yang, Y., Wei, X.-J. & Liu, J. Suitability of a thermoelectric power generator for implantable medical electronic devices. *J. Phys. D* **40**, 5790–5800 (2007).
7. Lay-Ekuakille, A., Vendramin, G., Trotta, A. & Mazzotta, G. Thermoelectric generator design based on power from body heat for biomedical autonomous devices. In *Proc. 2009 IEEE Int. Workshop Medical Meas. Appl., MeMeA* 1–4 (IEEE, 2009); https://doi.org/10.1109/MEMEA.2009.5167942
8. Rojas, J. P. et al. Review—Micro and nano-engineering enabled new generation of thermoelectric generator devices and applications. *ECS J. Solid State Sci. Technol.* **6**, N3036–N3044 (2017).
9. Leonov, V. & Vullers, R. J. M. Wearable electronics self-powered by using human body heat: the state of the art and the perspective. *J. Renew. Sustain. Energy* **1**, 062701 (2009).
10. Kim, S. J., We, J. H. & Cho, B. J. A wearable thermoelectric generator fabricated on a glass fabric. *Energy Environ. Sci.* **7**, 1959–1965 (2014).
11. Kishi, M. et al. Fabrication of a miniature thermoelectric module with elements composed of sintered Bi-Te compounds. In *Proc. ICT'97, 16th Int. Conf. Thermoelectrics (cat. no. 97TH8291)* 653–656 (IEEE, 1997); https://doi.org/10.1109/ICT.1997.667614
12. Fleurial, J.-P. et al. Thermoelectric microcoolers for thermal management applications. In *Proc. ICT'97, 16th Int. Conf. Thermoelectrics (cat. no. 97TH8291)* 641–645 (IEEE, 1997); https://doi.org/10.1109/ICT.1997.667611
13. Birkholz, U., Fettig, R. & Rosenzweig, J. Fast semiconductor thermoelectric devices. *Sens. Actuat.* **12**, 179–184 (1987).
14. Böttner, H. et al. New thermoelectric components using microsystems technologies. *J. Microelectromech. Syst.* **13**, 414–420 (2004).
15. Bahk, J. H., Fang, H., Yazawa, K. & Shakouri, A. Flexible thermoelectric materials and device optimization for wearable energy harvesting. *J. Mater. Chem. C* **3**, 10362–10374 (2015).
16. Wendt, H. & Kreysa, G. *Electrochemical Engineering: Science and Technology in Chemical and Other Industries* (Springer, Berlin, Heidelberg, 1999).
17. Schumacher, C. et al. Optimization of electrodeposited p-doped Sb_2Te_3 thermoelectric films by millisecond potentiostatic pulses. *Adv. Energy Mater.* **2**, 345–352 (2012).
18. Schumacher, C. et al. Optimizations of pulsed plated p- and n-type Bi_2Te_3-based ternary compounds by annealing in different ambient atmospheres. *Adv. Energy Mater.* **3**, 95–104 (2013).
19. Snyder, G. J., Lim, J. R., Huang, C.-K. & Fleurial, J.-P. Thermoelectric microdevice fabricated by a MEMS-like electrochemical process. *Nat. Mater.* **2**, 528–531 (2003).
20. Enright, R. et al. Electrodeposited micro thermoelectric module design for hybrid semiconductor laser cooling on a silicon photonics platform. *Trans. Electrochem. Soc.* **69**, 37–51 (2015).
21. Medina-Sánchez, M. & Schmidt, O. G. Medical microbots need better imaging and control. *Nature* **545**, 406–408 (2017).
22. Stordeur, M. & Stark, I. Low power thermoelectric generator — self-sufficient energy supply for micro systems. In *Proc. ICT'97, 16th Int. Conf. Thermoelectrics (cat. no.97TH8291)* 575–577 (IEEE, 1997); https://doi.org/10.1109/ICT.1997.667595
23. Fleurial, J. P. et al. Development of thick-film thermoelectric microcoolers using electrochemical deposition. In *Thermoelectr. Mater. 1998 — Next Gener. Mater. Small-Scale Refrig. Power Gener. Appl.* Vol. 545 (eds Tritt, T. M. et al.) 493–500 (1999).
24. da Silva, L. W. & Kaviany, M. Fabrication and measured performance of a first-generation microthermoelectric cooler. *J. Microelectromech. Syst.* **14**, 1110–1117 (2005).
25. Lim, J. R. et al. Fabrication method for thermoelectric nanodevices. *Adv. Mater.* **17**, 1488–1492 (2005).
26. Huang, I.-Y., Li, M.-J., Chen, K.-M., Zeng, G.-Y. & She, K.-D. Design and fabrication of a column-type microthermoelectric cooler with bismuth telluride and antimony telluride pillars by using electroplating and MEMS technology. In *2007 2nd IEEE Int. Conf. Nano/Micro Eng. Molecular Syst.* 749–752 (IEEE, 2007); https://doi.org/10.1109/NEMS.2007.352126
27. Gross, A. J. et al. Multistage planar thermoelectric microcoolers. *J. Microelectromech.Syst.* **20**, 1201–1210 (2011).
28. Kim, M.-Y. & Oh, T.-S. Thermoelectric thin film device of cross-plane configuration processed by electrodeposition and flip-chip bonding. *Mater. Trans.* **53**, 2160–2165 (2012).
29. Roth, R. et al. Design and characterization of micro thermoelectric cross-plane generators with electroplated Bi_2Te_3, Sb_xTe_y, and reflow soldering. *J. Microelectromech. Syst.* **23**, 961–971 (2014).
30. Zhang, W., Yang, J. & Xu, D. A high power density micro-thermoelectric generator fabricated by an integrated bottom-up approach. *J. Microelectromech. Syst.* **25**, 744–749 (2016).
31. Trung, N. H., Van Toan, N. & Ono, T. Fabrication of π-type flexible thermoelectric generators using an electrochemical deposition method for thermal energy harvesting applications at room temperature. *J. Micromech. Microeng.* **27**, 125006 (2017).
32. Yang, F., Zheng, S., Wang, H., Chu, W. & Dong, Y. A thin film thermoelectric device fabricated by a self-aligned shadow mask method. *J. Micromech. Microeng.* **27**, 055005 (2017).
33. Lin, S. et al. Tellurium as a high-performance elemental thermoelectric. *Nat. Commun.* **7**, 10287 (2016).
34. Younes, E., Christofferson, J., Maize, K. & Shakouri, A. Short time transient behavior of SiGe-based microrefrigerators. *MRS Proc.* **1166**, 1166–N01-06 (2009).

35. He, R., Schierning, G. & Nielsch, K. Thermoelectric devices: a review of devices, architectures, and contact optimization. *Adv. Mater. Technol.* **2017**, 1700256 (2017).
36. Garcia, J. et al. JSS focus issue on thermoelectric materials and devices fabrication and modeling of integrated micro-thermoelectric cooler by template-assisted electrochemical deposition. *ECS J. Solid State Sci. Technol.* **6**, 3022–3021 (2017).
37. Snyder, G. J. & Toberer, E. S. Complex thermoelectric materials. *Nat. Mater.* **7**, 105–114 (2008).
38. Muñoz-García, M. A., Moreda, G. P., Raga-Arroyo, M. P. & Marín-González, O. Water harvesting for young trees using Peltier modules powered by photovoltaic solar energy. *Comput. Electron. Agric.* **93**, 60–67 (2013).
39. Rowe, D. M. in *CRC Handbook of Thermoelectrics* 1251–1256 (CRC, New York, 1995).
40. Perron, J. C. Thermal conductivity of selenium-tellurium liquid alloys. *Phys. Lett. A* **32**, 169–170 (1970).
41. Nolas, G. S., Sharp, J. & Goldsmid, H. J. *Thermoelectrics: Basic Principles and New Materials Developments* (Springer, Berlin Heidelberg, 2001).

Acknowledgements

The authors thank T. Sieger, H. Stein, C. Kupka and R. Uhlemann in IFW Dresden for helpful technical support. G.L. thanks T. G. Woodcock in Leibniz IFW Dresden for his valuable comments and suggestions for this Article. G.L. and V.B acknowledge financial support from the European Union (EU) and the Free State of Saxony through the European Regional Development Fund (ERDF) (SAB GroTEGx, grant no. 100245375). J.G.F. acknowledges financial support from the EU's Horizon 2020 research and innovation program (H2020 RIA Tips, grant no. 644453), D.A.L.R. acknowledges funding from the Mexican National Council for Science and Technology (grant no. CVU611106).

Author contributions

G.L., J.G.F., H.R., G.S. and K.N. designed the work. G.L. and J.G.F. fabricated the integrated microcoolers and carried out the device performance characterization. J.G., D.A.L.R. and V.B. performed the model simulation based on FEM COMSOL and analytical calculations. G.L. and N.P. performed the scanning electron microscope observations. G.L. and I.S. carried out the temperature-dependent cooling performance measurements. G.L. wrote the manuscript, with input from all authors.

Competing interests

The authors declare no competing interests.

Additional information

Supplementary information is available for this paper at https://doi.org/10.1038/s41928-018-0148-3.

Reprints and permissions information is available at www.nature.com/reprints.

Correspondence and requests for materials should be addressed to G.L.

Publisher's note: Springer Nature remains neutral with regard to jurisdictional claims in published maps and institutional affiliations.